scientific reports

Check for updates

OPEN

Impact scenarios on groundwater availability of southern Italy by joint application of regional climate models (RCMs) and meteorological time series

Daniele Lepore[1]✉, Edoardo Bucchignani[2], Myriam Montesarchio[2], Vincenzo Allocca[1], Silvio Coda[1], Delia Cusano[1] & Pantaleone De Vita[1]

Nowadays the phenomenon of global warming is unequivocal, as confirmed by the latest reports of the IPCC and studies of the climate-change impacts on ecosystems, global economy, and populations. The effect of climate change on groundwater is a very relevant task especially for regions dependent chiefly on groundwater availability, as for the southern Italy. In such a territorial framework, to achieve a detailed hydro-climatological characterization, an Ensemble of 15 RCMs (E15) derived from the EURO-CORDEX project was analyzed considering two IPCC Representative Concentration Pathways (RCP4.5 and RCP8.5). The E15 was calibrated over the period (1950–1996) by a statistical comparison with data observed by the regional meteorological network managed by the former National Hydrological Service (SIMN), Department of Naples. The effects of climate change on air temperature (T), precipitation (P) and, consequently, on actual evapotranspiration (ETR) and effective precipitation Pe (P – ETR) were analyzed until 2100. The latter was considered as a proxy of groundwater recharge of the principal aquifer systems, represented chiefly by the karst aquifers. As a principal result, it was found that the E15 is basically able to reproduce the observed annual precipitation (OBS_P) and mean annual air temperature (OBS_T), being characterized by a very similar frequency distribution. Accordingly, an inferential statistical approach was performed for calibrating E15 precipitation ($E15_P$) and air temperature ($E15_T$) based on the compensation of the difference with OBS_P (+ 7%) and OBS_T (– 16%). The E15 projects a reduction in precipitation and an increase in air temperature under both RCPs, with a divergence point between the two scenarios occurring by about 2040. As a principal result, Pe shows declining trends for both RCP scenarios, reaching a decrease of the 11-yrs moving average down to – 20%, for RCP4.5, and – 50%, for RCP8.5, even if characterized by relevant inter-annual fluctuations.

Keywords Groundwater recharge, Karst aquifers, RCMs, Southern Italy

The economic and social development of southern Italy is fundamentally sustained by the availability of groundwater resources, which are provided by a series of principal aquifers. Among these aquifers, the karst ones are the most significant due to their high mean annual groundwater yield, which is the highest in Europe[1]. In such a framework, the study of the future effects of climate change on groundwater recharge and availability is a very relevant task.

Precipitation and air temperature represent the key variables controlling groundwater recharge processes and the most susceptible to the effects of climate change. As highlighted by various researches, the effects of climate change will substantially disrupt the water cycle, leading to an increase in the air temperature and in the intensity and frequency of extreme hydro-climatic events in numerous regions worldwide[2–5]. The Mediterranean region,

[1]Department of Earth, Environmental and Resource Sciences (DiSTAR), University of Naples Federico II, 80126 Naples, Italy. [2]Meteorology Laboratory, Centro Italiano Ricerche Aerospaziali (CIRA), 81043 Capua, Italy. ✉email: daniele.lepore@unina.it

where Italy occupies the central part, is acknowledged as one of the major climate change hotspots due to future projections of air temperature increase and annual precipitation decrease[6–8].

One of the most recognized approaches for the development of future climate projections is based on the usage of regional climate models (RCMs) under different greenhouse gas emission scenarios[9]. Despite the important relationship between climate patterns and groundwater resources[10], researches have not advanced yet the analysis of the future impacts of climate change on groundwater recharge processes to the same extent of those carried out on surface water resources[11]. Consequently, the analysis of future hydrogeological scenarios, depending on long-term patterns of precipitation and air temperature, appears as a fundamental achievement for a resilient management of groundwater resources in southern Italy, where the economic development is mainly reliant on groundwater resources and studies regarding the impacts of climate change are still scarce.

Accordingly, this study aims to analyse the effects of the climate change on the groundwater recharge processes of the major aquifers systems of the southern Italy, by the application of data of 15 RCMs provided by the European Coordinated Regional Downscaling Experiment (EURO-CORDEX)[7], which are currently used to project scenarios of precipitation (P) and air temperature (T) until the end of the XXI century. Moreover, in this study we propose a novel and practical method for the evaluation and correction of different RCMs' data against observed historic meteorological time series (1950–1996) over southern Italy, which is based on an inferential statistical approach. The estimation of expected changes in annual values of actual evapotranspiration (ETR) and effective precipitation (Pe) until 2100 was obtained by considering an ensemble mean of 15 RCMs (E15) under two representative concentration pathways scenarios, respectively IPCC RCP 4.5 and RCP 8.5[5,12]. The proposed approach of the bias correction of RCMs is performed at the annual time-scale, and is based on the comparison at the regional scale with time series recorded by a national meteorological network, which functioned discontinuously in space and time.

To the best of our knowledge, the outcomes of the present research provide a relevant contribution for the first time in the assessment of groundwater resources availability under future water crisis scenarios in southern Italy.

The results of the analyses are addressed primarily to the karst aquifers, which represent the most important sources of groundwater for the region, but secondarily also to the others minor aquifers which represent local relevant groundwater resources.

RCMs in the Mediterranean area

General circulation models (GCMs) and RCMs are applied worldwide at different spatial resolutions and temporal scales, for the development of climate scenarios up to the end of the current century. A series of international projects and studies (e.g. CORDEX[7]) have produced a huge ensemble of climate projections, accounting for most of the uncertainties affecting climate change predictions[13]. At the resolution of GCMs Italy is not well delineated, since it has a complex topography, ranging from high mountain chains to a diverse coastline. For this reason, data from high-resolution RCMs have been considered in the present research. Specifically, Holman[14] suggested that the best practice for using climate projections to assess the impact on groundwater resources was to consider multiple RCMs driven by multiple GCMs under different emission scenarios (pathways). This approach introduces additional variability in the climate data, which enhances uncertainty in the assessment of future groundwater recharge[15].

As first step, the state of art of RCMs simulations (and related driving GCMs) available in the framework of Mediterranean karst aquifers has been investigated. It is summarized in Table 1, where a list of GCMs/RCMs combination is shown, along with relevant information (e.g. spatial and temporal resolution of the models scenarios).

Some of the RCMs applied derive from ENSEMBLES and PRUDENCE projects, under the A1B scenario, defined by IPCC in the Special Report on Emissions Scenarios (SRES)[24].Other RCMs applied derive from the EURO-CORDEX project[25]. The EURO-CORDEX team performed a dynamical downscaling of the global simulations from the Coupled Model Intercomparison Project Phase 5 (CMIP5) long-term experiments.

Year	Locations	GCMs/RCMs project	No of GCMs/RCMs	RCMs resolution km × km	Scenarios	Variables	Bias correction	Groundwater recharge quantification methods	Reference
2012	Spain	ENSEMBLES	3	25	A1b	T, P	Yes	E	16
2014	Spain	ENSEMBLES	3	25	A1b	T, P	Yes	E	17
2015	Spain	PRUDENCE ENSEMBLES	7	22–50	A1b A2	T, P	Yes	C	18
2018	Spain	CORDEX	9	12.5	RCP8.5	T, P	Yes	E	19
2019	Italy	EURO-CORDEX	13	12.5	RCP4.5 RCP8.5	T, P	Yes	N	20
2019	Spain	EURO-CORDEX	9	12.5	RCP8.5	T, P	Yes	E	21
2020	Greece	EURO-CORDEX	11	12.5	RCP 2.6 RCP4.5 RCP8.5	T, P	Yes	N	22
2021	Greece	EURO-CORDEX	8	12.5	RCP4.5 RCP8.5	T, P	Yes	N	23

Table 1. Literature applications of GCMs/RCMs in the framework Mediterranean areas. *P* precipitation; *T* air temperature; *E* empirical; *N* numerical; *C* combined.

They are based on greenhouse gas scenarios (representative concentration pathways, RCPs) corresponding to stabilization of radiative forcing after the twenty-first century at 4.5 W/m^2 (RCP4.5), rising radiative forcing crossing 8.5 W/m^2 at the end of twenty-first century (RCP8.5), and peaking radiative forcing within the twenty-first century at 3.0 W/m^2 and declining afterwards (RCP2.6)[26].

Precipitation and air temperature are the fundamental environmental variables controlling climate and groundwater recharge processes, whose time series, simulated by the RCMs, are easily and largely applicable for the quantification of the groundwater recharge by empirical and numerical models. Ensembles of different GCMs/RCMs are recognized as a suitable approach for reducing the uncertainty of the results given by a single model[27,28]. For the same scope, temporal analyses are carried out at various time scales for a better assessment. Statistical downscaling techniques can increase further the spatial resolution of climate data up to the local scale, while a range of bias correction methods[28,29] have been developed to overcome the large biases in climate models, and can be used also for the quantification of the groundwater recharge through empirical models or water budget approach.

Data and methods

Study area description

The territory of southern Italy is characterized by a high heterogeneity and complexity of geological-structural and hydrogeological features. The principal hydrogeological features of the southern Italy can be summarized in nine hydrogeological domains[30] which, in decreasing order of relevance for what regards the mean annual specific groundwater yield (Fig. 1), can be identified as: (a) Mesozoic carbonate series that, depending on hydrogeological features, can be arranged in four subgroups: calcareous-siliceous, limestone, dolomitic, carbonate and Apulian foreland carbonate aquifers; (b) Plio-Quaternary alluvial and epiclastic deposits; (c) volcanic rocks and soils of Plio-Quaternary eruptive centres; (d) Paleozoic crystalline-metamorphic rocks of the Calabrian arch; (e) Cretaceous-Cenozoic basin series, which mainly constitute the minor mountainous or hilly reliefs of the southern Apennines.

In such interregional framework, the study area includes the entire portion of the western sector of the southern Apennines (about 19,339 km^2), where Mesozoic carbonate series, forming high mountain ranges,

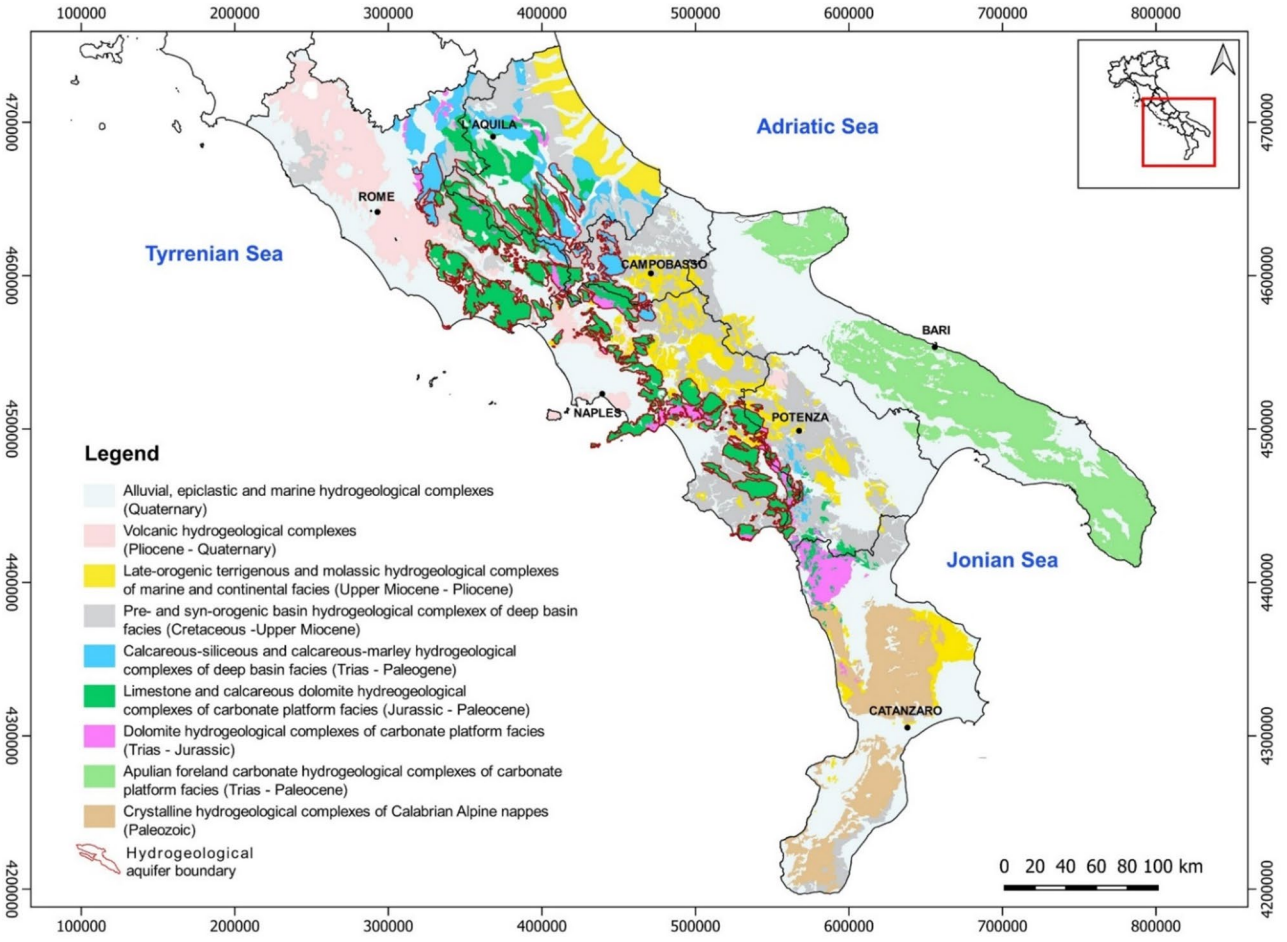

Figure 1. Hydrogeological map of the continental southern Italy showing the nine principal hydrogeological domains[30]. Hydrogeological boundaries of karst aquifers are also shown. The map was created using QGIS software (v. 3.34; https://qgis.org/).

outcrop and constitute very extended karst aquifers characterized by high permeability due to fracturing and karst phenomena (Fig. 1). These karst aquifers are characterized by limestone, limestone-dolomite and dolomite rocks, ranging in age from Triassic to Upper Cretaceous, derived from the tectonic disintegration of the carbonate platform that occurred during the Miocene tectonic phases[31,32]. In southern Italy, karst aquifers cover the 45%[33] of the territory hosting the major groundwater resources which supply drinkable, industrial and thermos-mineral uses as well as contributing to the equilibrium of river ecosystems. This is favoured by the peculiar geological-structural, hydrogeological, geomorphological and climatological settings of the region which determine the occurrence of several high-permeability karst aquifers, with a high mean annual groundwater recharge and circulation rates.

Given their importance, many studies have been carried out on the karst aquifers of southern Italy regarding: (i) hydrogeological characterization and the mapping of groundwater resources[30,34,35]; (ii) groundwater recharge estimation at the different spatio-temporal scales and by terrestrial and satellite datasets[33,36–38]; (iii) groundwater vulnerability to pollution[39,40], microbial contamination and environmental impact of cattle grazing on karst groundwater[41]. The Plio-Quaternary deposits, which include deposits of alluvial plains, coastal plains and intermontane basins, outcropping for about 24,500 km^2, which are directly recharged by effective or secondary infiltration from watercourses, thus receiving lateral groundwater inflow from the adjoining karst aquifer systems.

The lateral confinement of karst aquifers by low-permeability terrains constrains the groundwater circulation toward huge basal springs which are often characterized by high flows up to a few m^3/s[34,42,43], and predisposed to the effective tapping. Therefore, karst aquifers represent the main source of groundwater for southern Italy, providing an estimated average annual water volume of approximately $4100 \times 10^6\ m^3 \cdot year^{-1}$ with a mean specific annual groundwater yield up to $0.035\ m^3 \cdot s^{-1} \cdot km^{-2}$.[30]

The principal regional aqueducts are supplied by the tapping by gravity of the main basal springs of karst aquifers, in most cases not provided by pumping systems, therefore the availability of groundwater resources of these aquifers correspond to their natural recharge.

Climate models

To investigate the future climate projections and the related impacts on groundwater recharge processes over the study area (Fig. 2), annual precipitation and mean air temperature data from the EURO-CORDEX simulations[25] were achieved from the nodes of the earth system grid federation (ESGF).

Specifically, 15 different combinations of GCMs/RCMs were selected (Table 2). RCMs selected belong to the subset EUR-11 with a resolution of 0.11° (about 12.5 km) (Fig. 2b). Accordingly, data available for the "historical experiment" period (from 1950/1970 to 2005) and scenarios (from 2006 to 2099/2100) were analysed in this research. As already mentioned, RCP4.5 and RCP8.5 scenarios were selected, being the RCP8.5 the most severe ("business as usual"), while the RCP4.5 is representative of intermediate conditions.

According to other studies developed with a general purpose and in different geographical frameworks[44–48], the RCP 8.5 is commonly used because representing the most extreme conditions, even if being the least likely[49]. As a result, an ensemble of 15 RCM_S (E15; Table 2) was reconstructed, re-projected in WGS84-UTM 33N and analysed.

Observed precipitation and air temperature time series (1950–1996)

In the southern Italy, as well as for the rest of the national territory, a hydrological monitoring has been carried out since 1921 by means of a dense monitoring network, managed by the SIMN governmental agency and consisting in a numerous series of rain gauges and air temperature stations.

In the study area, the management of the monitoring network was in charge of the Department of Naples of the SIMN, which operated in a territory covering a large part of southern Italy, comprising the study area (Fig. 2a). The meteorological monitoring network was provided initially by mechanical rain gauges, based on the accumulation of the daily rainfall, and air temperature stations.

Starting from 1921, the number of rain gauges and air temperature stations was progressively increased and improved technologically until reaching a total of 423 stations in 1999. The recorded data, after a process of validation, were published in the annals by the aggregation of data from daily, to monthly and annual temporal scales.

The meteorological network undergone different changes during the period 1921–1999 due to the progressive increase of the number of stations as well as their discontinuous activity, because of temporary malfunctioning or abandonment during the World War II as well their relocation. These continuous changes of the monitoring network resulted in time series discontinuous in space and time.

Notwithstanding these issues, the huge database of historical meteorological data was considered very relevant for the comparison with RCMs data of the "historical experiments" periods (from 1950/1970 to 2005) and innovative for the regional scale of analysis, instead of the more common site-specific one, as well as challenging for its discontinuous functioning in space and time. Therefore, annual precipitation and mean annual air temperature were extracted by the annals of the SIMN, made of public access by a dedicated project of Italian Institute for Environmental Protection and Research (ISPRA), and filed in a database covering the period 1950–1996. In detail, annual precipitation and mean annual air temperature data were extracted for each of the available monitoring stations, which were considered as observation points (OBS). The OBS data were used for a statistical comparison to the E15 ones at the regional scale, by considering both types of data comprised in each of the grid cells of the RCMs (~ 12 km) (Fig. 2a and b). A total of 143 RCMs grid cells were recognized comprising rain gauge stations, while 96 air temperature stations.

In order to represent the spatial and temporal variability of rain gauge and air temperature stations comprised in the cells of the RCMs, a representation in the form of heat map was carried out respectively (Figs. 3 and 4).

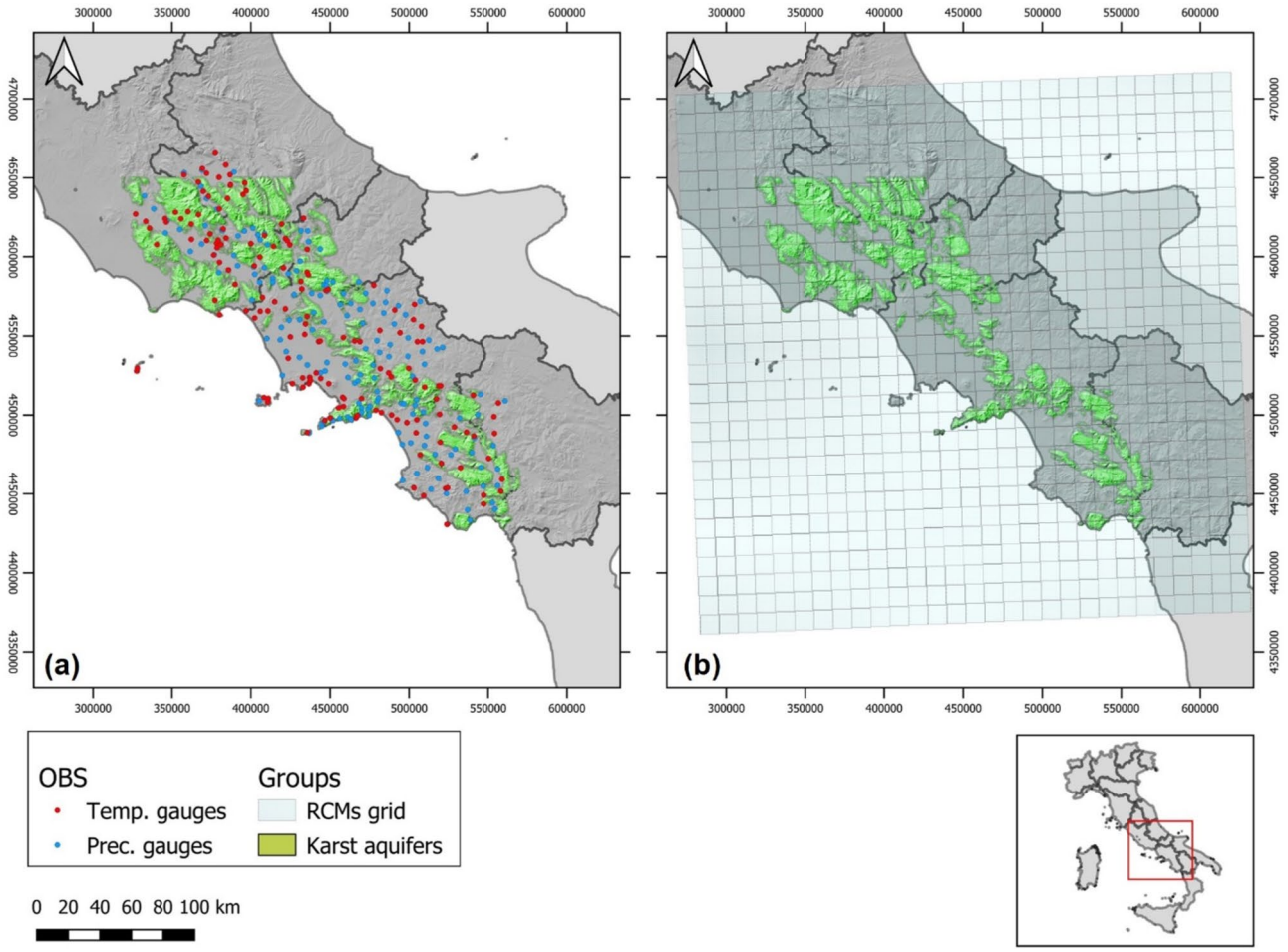

Figure 2. (**a**) Map of the modelled study area showing the distributions of air temperature and rain gauge stations (OBS) which functioned, even discontinuously, in the calibration period (1950–1996); (**b**) EUR-11 RCMs grid. Karst aquifers (green colour) of the southern Apennines area also shown in both maps. The maps were created using QGIS software (v. 3.34; https://qgis.org/).

Domain	Institution	GCM	RCM	Historical	RCP4.5	RCP8.5
EUR-11	CLMcom-BTU	MPI-ESM-LR	CCLM4-8-17	1949–2005	2006–2100	2006–2100
	CLMcom	HadGEM2-ES	CCLM4-8-17	1949–2005	2006–2099	2006–2099
		EC-EARTH	CCLM4-8-17	1949–2005	2006–2100	2006–2100
		CNRM-CM5	CCLM4-8-17	1950–2005	2006–2100	2006–2100
	KNMI	CNRM-CM5	RACMO22E	1950–2005	2006–2100	2006–2100
		EC-EARTH	RACMO22E	1950–2005	2006–2100	2006–2100
		HadGEM2-ES	RACMO22E	1950–2005	2006–2099	2006–2099
	DMI	EC-EARTH	HIRHAM5	1951–2005	2006–2100	2006–2100
		HadGEM2-ES	HIRHAM5	1951–2005	2006–2099	2006–2099
		NorESM1-M	HIRHAM5	1951–2005	2006–2100	2006–2100
	SMHI	CNRM-CM5	RCA4	1970–2005	2006–2100	2006–2100
		EC-EARTH	RCA4	1970–2005	2006–2100	2006–2100
		IPSL-CM5A-MR	RCA4	1970–2005	2006–2100	2006–2100
		HadGEM2-ES	RCA4	1970–2005	2006–2099	2006–2099
		MPI-ESM-LR	RCA4	1970–2005	2006–2100	2006–2100

Table 2. EURO-CORDEX models selected and adopted in the study area to be considered for the reference ensemble (E15). EUR-11 indicate models at resolution of 0.11° (about 12.5 km).

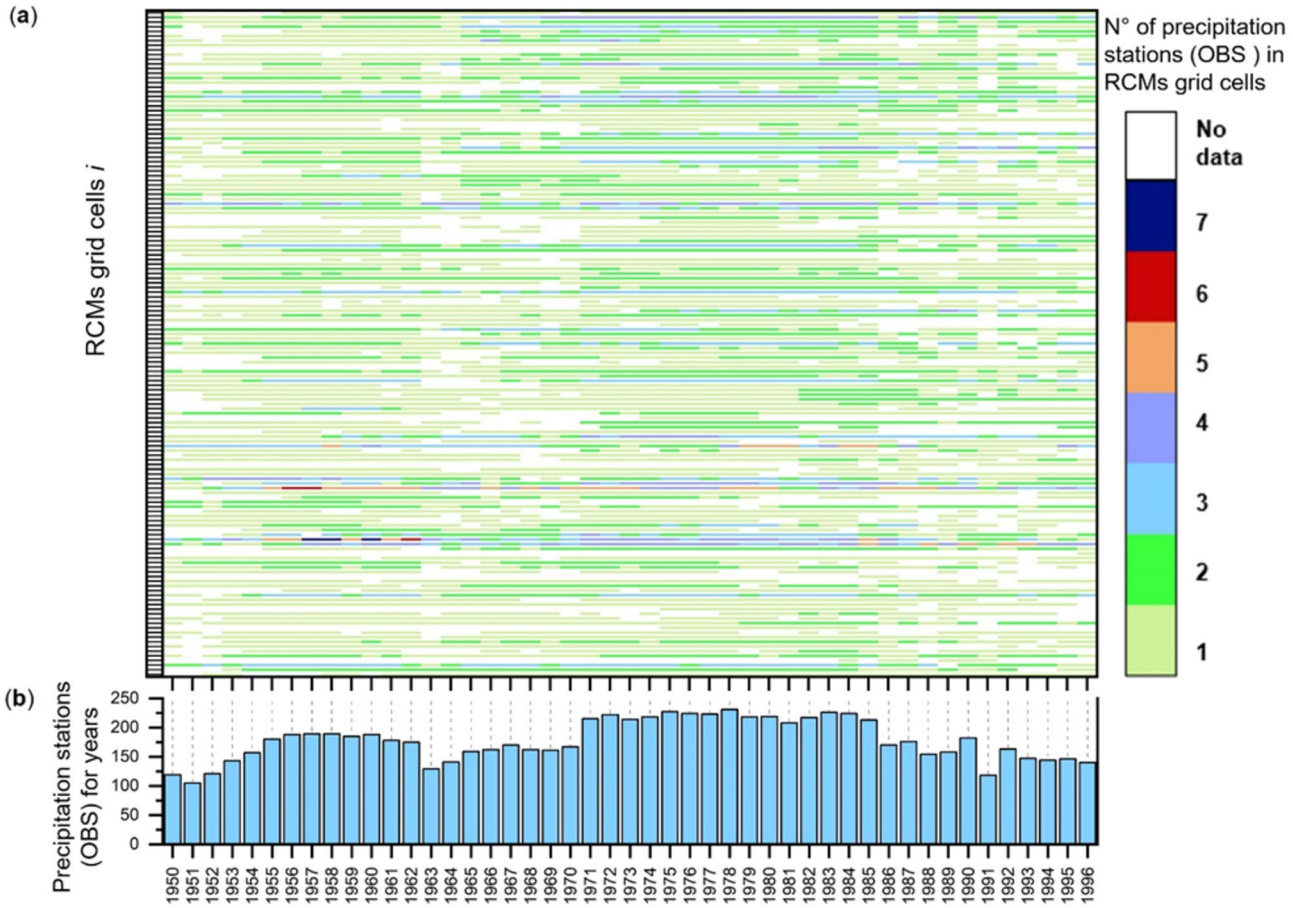

Figure 3. Spatio-temporal variation of the precipitation data across the study area: (**a**) temporal variation of the number of precipitation stations (OBS) occurred in the period 1950–1996 in grid cells *i* of the RCMs; (**b**) total number of precipitation stations (OBS) for each year.

By the analysis of spatial and temporal distribution of rain gauges in the grid cells of RCMs (Fig. 2b) a minimum number of 100 functioning rain gauges in 1951 and 1991 and a maximum of 225 in 1978 was recognized (Fig. 3). The coverage of each grid cell of RCMs with at the least one rain gauge, up to six, prevails on cells with no rain gauges.

Regarding the spatial and temporal distribution of air temperature stations in the grid cells of RCMs (Fig. 4), the minimum number of 20 occurred in 1950 and a maximum of 96 in 1985. The coverage of each cell with no air temperature stations prevails on those comprising at least one. The latter were recognized encompassing up to four air temperature stations for each grid cell. The lower spatial density of air temperature stations in comparison to that of rain gauges is due to the lower spatial variability of the air temperature which is mostly controlled by the altitude only.

RCMs processing: bias assessment and correction

All the RCM_S data (precipitation and air temperature) were pre-processed with the climate data operators (CDO) software[50], which is a collection of operators and tools for standard processing of climate and forecast model data in NetCDF format. The operators include arithmetic functions, data selection and subsampling tools and spatial interpolation.

For each model, the pre-processing has involved the aggregation of the NetCDF datasets and the conversion of the units of precipitation (from $kg \cdot m^2 \cdot s^{-1}$ to $mm \cdot h^{-1}$) and air temperature (from K to °C). Furthermore, the precipitation and air temperature data from RCMs (based on a 360-day calendar) were adjusted by linear interpolation to align with the standard Gregorian calendar. Therefore, a subset of data related to the area of the southern Apennines was extracted (Fig. 2b).

RCMs data need the application of a bias correction technique, aimed to the removal of systematic errors. Which is performed considering a period in which observed (OBS) and modelled time series are available and overlapped[9].

Different methodologies for the bias correction have been developed and are available in literature[28], depending on the choice of the method on both the type of the observed data available and the goal of the study[9].

Bias-correction methods require daily or monthly time-series over a period of at least 30 years[51]. The purpose of this stage of data processing was to assess the differences existing between the RCM_S "historical experiments"

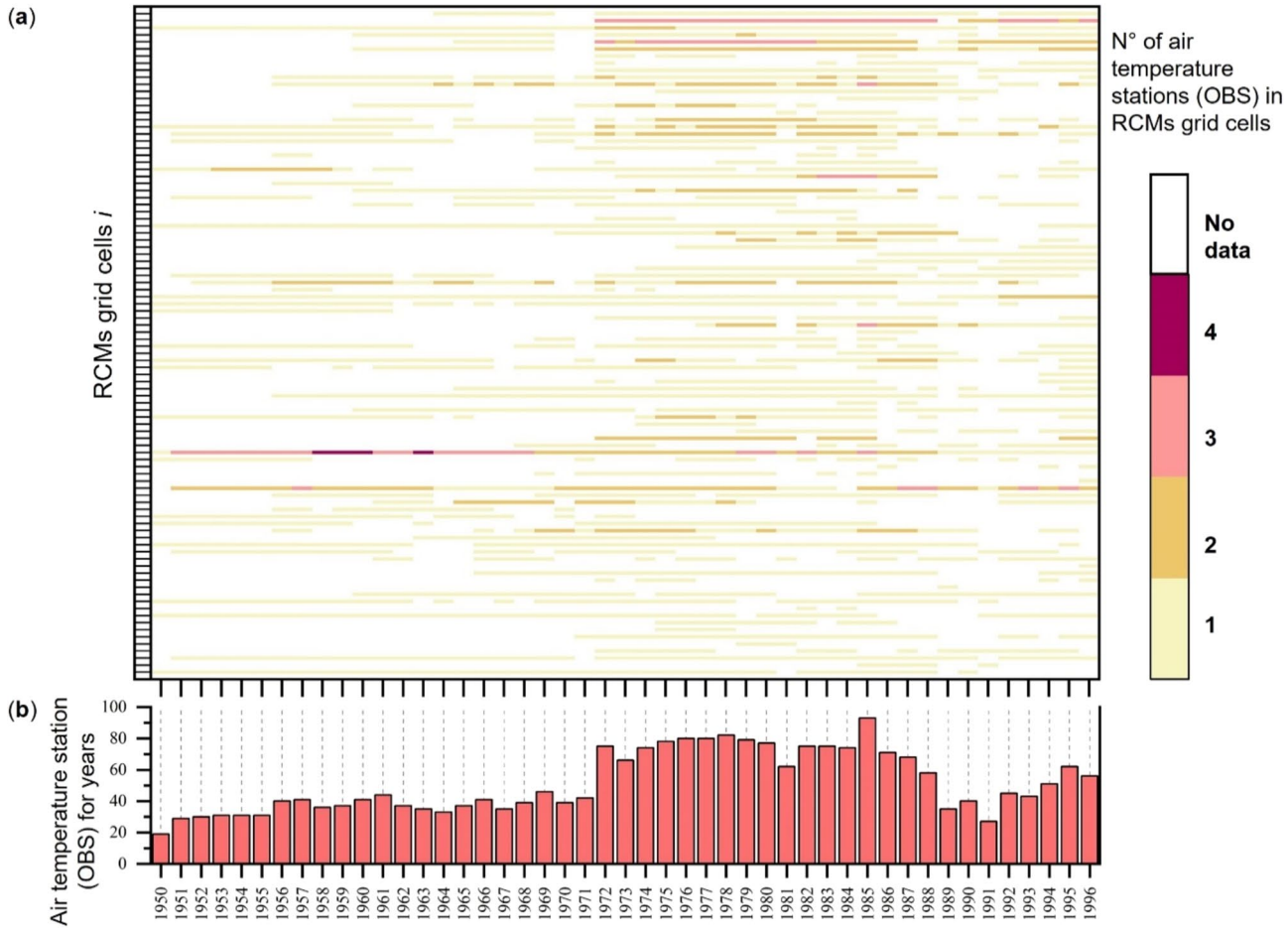

Figure 4. Spatio-temporal variation of the air temperature data: (**a**) temporal variation of the number of air temperature stations (OBS) occurred in the period 1950–1996 in grid cells *i* of the RCMs; (**b**) total number of air temperature stations (OBS) for each year.

datasets and the measured data (OBS) in the considered period (1950–1996). Data elaboration was performed with the high-level functions NetCDF Library Package of MATLAB® (R2021b) applicable for reading and processing climate variables from NetCDF data files. Specifically, a method based on inferential statistical studies of the bias was adopted. In order to allow the comparison between the E15 and OBS data, two pairs of datasets were created, based on the recognition of grid cells of the RCM model within which OBS precipitation (OBS_P) and OBS air temperature (OBS_T) resulted available (Fig. 5a and b).

For each year, OBS_P and OBS_T given at each grid cell were compared with the E15 precipitation ($E15_P$) and air temperature ($E15_T$) data related to the same grid cell (Fig. 5a and b). In the case of multiple stations occurring in the same grid cell, mean values of OBS_P and OBS_T were calculated and compared with the corresponding $E15_P$ and $E15_T$ data. The *bias* analysis between $E15_P$ and OBS_P and between $E15_T$ and OBS_T was carried for every grid cell at the annual scale by the equation Eq. (1):

$$Bias_{P,T,t}(j) = \frac{(Model_{P,T,t}(j) - OBS_{P,T,t}(j))}{OBS_{P,T,t}(j)}, \tag{1}$$

where $Model_{P,T,t}(j)$ is the value of $E15_P$ or $E15_T$ and $OBS_{P,T,t}(j)$ is the observed value of precipitation or air temperature for the year t ($t = 1950, 1951 \ldots 1996$) in the *jth* grid cell.

Then, the mean value of the bias over the generic t_{year} ($\overline{Bias_{P,T,t}}$) and the whole area, was calculated by Eq. (2):

$$\overline{Bias_{P,T,t}} = \frac{\sum_{j=1}^{n} Bias_{P,T}(j)}{\sum_{j=1}^{n} j}, \tag{2}$$

In which n indicates the number of grid cells considered. Finally, the bias-corrected annual value of the E15 ($Model^*_{P,T,t}(j)$) is then evaluated by Eq. (3):

$$Model^*_{P,T,t}(j) = Model_{P,T,t}(j) \times \left(1 - \overline{Bias_{P,T}}\right). \tag{3}$$

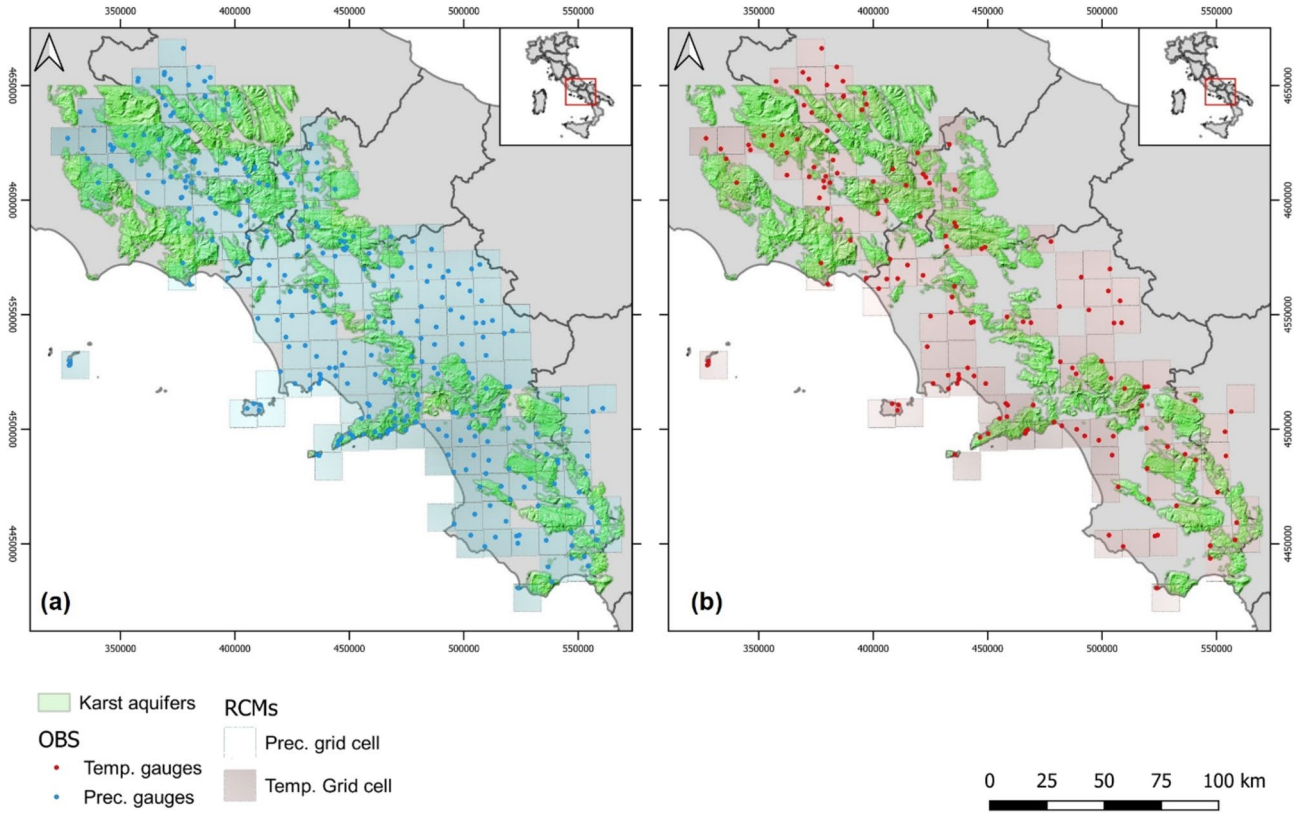

Figure 5. (**a**) rain gauges and (**b**) air temperature stations which functioned in the calibration period 1950–1996. The RCMs grid cells which comprised at least one monitoring station are also represented. The maps were created using QGIS software (v. 3.34; https://qgis.org/).

Hydro-climatological scenarios

The evaluation of the long-term effects of climate change on hydrological variables controlling groundwater recharge of karst aquifers was carried out considering the E15 bias-corrected values of precipitation and air temperature. Among the different hydrogeological domains, the spatial analyses were carried out on the areas of karst aquifers (Fig. 2a and b), which were considered the most relevant for the assessment of the impact of climate change on groundwater recharge due to their hydrogeological relevance. Accordingly, all the E15 grid cells intersecting the boundaries of the karst aquifers were extracted from the whole E15 dataset, and time series of mean annual precipitation and air temperature were created for reconstructing a complete time series including both the "historical experiment" period (1950–2005) and scenarios (2006–2100) under both the RCP4.5 and RCP8.5 pathways.

The evaluation of the climate change impact on groundwater recharge was assessed through the application of the hydrological budget equation Eq. (4):

$$P_{tj} = ETR_{tj} + Ie_{tj} + R_{tj}, \tag{4}$$

where P_{tj} is the precipitation, ETR_{tj} is the actual evapotranspiration, Ie_{tj} is the effective infiltration or groundwater recharge and R_{tj} is the runoff, respectively related to the t_{year} and j_{cell}.

The ETR was estimated by the Turc empirical formula[52,53] Eq. (5):

$$ETR_{t,j} = \frac{P_{t,j}}{\sqrt{0.9 + \left(\frac{P_{t,j}}{300+25*T_{t,j}+0.05*T_{t,j}^3}\right)^2}}, \tag{5}$$

where $P_{t,j}$ is the total annual precipitation (mm) and $T_{t,j}$ is the mean annual air temperature (°C), both for the j_{cell}.

The Turc formula is commonly considered applicable to all different climates, either humid, arid, hot or cold because it was reconstructed by the application of the water balance equation to precipitation and runoff data of 254 drainage basins of Europe, Africa, America and the East Indies. In addition, the applicability of the Turc formula to the climate conditions of southern Italy has already been positively tested through a comparison with the results obtained by the other empirical formulas of Coutagne[54] and Thorntwaite[55] as well as with MODIS satellite estimations[33].

Since the Turc formula depends on the annual precipitation (P) and mean annual air temperature (T), it intrinsically incorporates the spatial heterogeneity of these two hydrological variables. Therefore, the formula was applied to all grid cells for which P and T data were reconstructed by the E15 for each year of the time series.

From Eqs. (4) and (5), the effective precipitation $Pe_{t,j}$ of the t_{year} and j_{cell} was considered as a proxy hydrological parameter describing the amount of precipitation potentially available groundwater recharge process and, therefore, useful for assessing the related effects of climate change scenarios Eq. (6):

$$Pe_{tj} = P_{tj} - ETR_{tj} = +Ie_{tj} + R_{tj}. \tag{6}$$

The reconstruction of Pe time series until 2100 is considered a fundamental step to assess the groundwater recharge by the application of empirical approach based on the multiplication by a factor known as Annual Groundwater Recharge Coefficient – AGRC[37], which is suitable at the annual and regional scales.

Finally, to investigate the variation of Pe relatively to the "historical experiment" period (1950–2005), the mean annual effective precipitation index (MAEPI)[56] was calculated for each year of the time series and the whole area, as follows Eq. (7):

$$MAEPI_t = \frac{Pe_t - PeHist_t}{PeHist_t}, \tag{7}$$

where $MAEPI_t$ is the Mean Annual Effective Precipitation Index for the t_{year} (%), Pe_t is the Effective Precipitation for the t_{year} and $PeHist_t$ is the Mean Annual Effective Precipitation of the whole E15 time series, corresponding to the "historical experiment" period (1950–2005), and the whole area.

Results

RCMs bias assessment

The bias assessment in the Calibration period (1950–1996), based on an inferential statistic approach, led to the quantification of RCMs accuracy in terms of precipitation and air temperature of the single RCMs considered (Table 2) against corresponding OBS, as well as between $E15_P$ and $E15_T$ and the OBS_P and OBS_T, respectively.

In detail, a total of 143 RCM_S grid cells were extracted for precipitation (Fig. 5a) and 96 for air temperature (Fig. 5b), considering in both cases only grid cells comprising monitoring stations. Table 3 shows RCMs bias values (mean, median and standard deviation) against the observed data for annual total precipitation and mean air temperature, averaged over the relative reference period. Figures 6 and 7 show the box plot representing the frequency distribution respectively of mean annual air temperature and precipitation of the 15 RCMs (before correction), the E15 and OBS. Although model values of single RCMs sometimes differ significantly from the corresponding OBS, a good accurate matching was found considering E15 values (Tables 4 and 5). In detail, the comparison of single RCMs with OBS reveals that HIRHAM5 and RCA4 showed the highest bias, while CCLM4-8-17 and RACMO22E the best accuracy.

Figure 8 shows the frequency distributions of OBS and E15 (before and after the correction). Both $E15_P$ and OBS_P were found statistically distributed with a log-normal model, showing an overestimation of $E15_P$ of about 7%. Conversely, air temperatures values of individual RCMs were recognized lower than the corresponding OBS values (Fig. 7), showing also a quite different statistical distribution for all RCM_S. The $E15_T$ values are generally 2 °C lower than OBS_T, and associated with the systematic errors of the RCMs. These air temperature biases were also observed in preceding studies carried out over the same region[45,57] and could be due to an

GCM	RCM	Reference period	Bias precipitation			Bias air temperature		
			Mean	Median	SD	Mean	Median	SD
MPI-ESM-LR	CCLM4-8-17	1950–1996	0.12	0.04	0.44	−0.13	−0.14	0.14
HadGEM2-ES	CCLM4-8-17	1950–1996	−0.14	−0.18	0.34	−0.08	−0.10	0.14
EC-EARTH	CCLM4-8-17	1950–1996	−0.09	−0.15	0.37	−0.18	−0.19	0.13
CNRM-CM5	CCLM4-8-17	1950–1996	0.02	−0.06	0.42	−0.16	−0.17	0.14
CNRM-CM5	RACMO22E	1950–1996	0.36	0.27	0.52	−0.25	−0.25	0.14
EC-EARTH	RACMO22E	1950–1996	0.09	0.03	0.41	−0.27	−0.27	0.14
HadGEM2-ES	RACMO22E	1950–1996	0.09	0.04	0.40	−0.16	−0.17	0.14
EC-EARTH	HIRHAM5	1951–1996	0.11	−0.10	0.83	−0.18	−0.17	0.13
HadGEM2-ES	HIRHAM5	1951–1996	−0.01	−0.19	0.74	−0.05	−0.05	0.14
NorESM1-M	HIRHAM5	1951–1996	0.07	−0.14	0.81	−0.06	−0.06	0.14
CNRM-CM5	RCA4	1970–1996	0.32	0.16	0.75	−0.19	−0.19	0.13
EC-EARTH	RCA4	1970–1996	0.08	−0.04	0.55	−0.23	−0.23	0.12
IPSL-CM5A-MR	RCA4	1970–1996	−0.08	−0.19	0.50	−0.15	−0.15	0.13
HadGEM2-ES	RCA4	1970–1996	0.05	−0.01	0.56	−0.12	−0.12	0.13
MPI-ESM-LR	RCA4	1970–1996	0.23	0.10	0.64	−0.13	−0.14	0.13

Table 3. RCMs bias values (mean, median and standard deviation) against observed data (OBS) for annual total precipitation (OBS_P) and mean air temperature (OBS_T), averaged over the relative reference period.

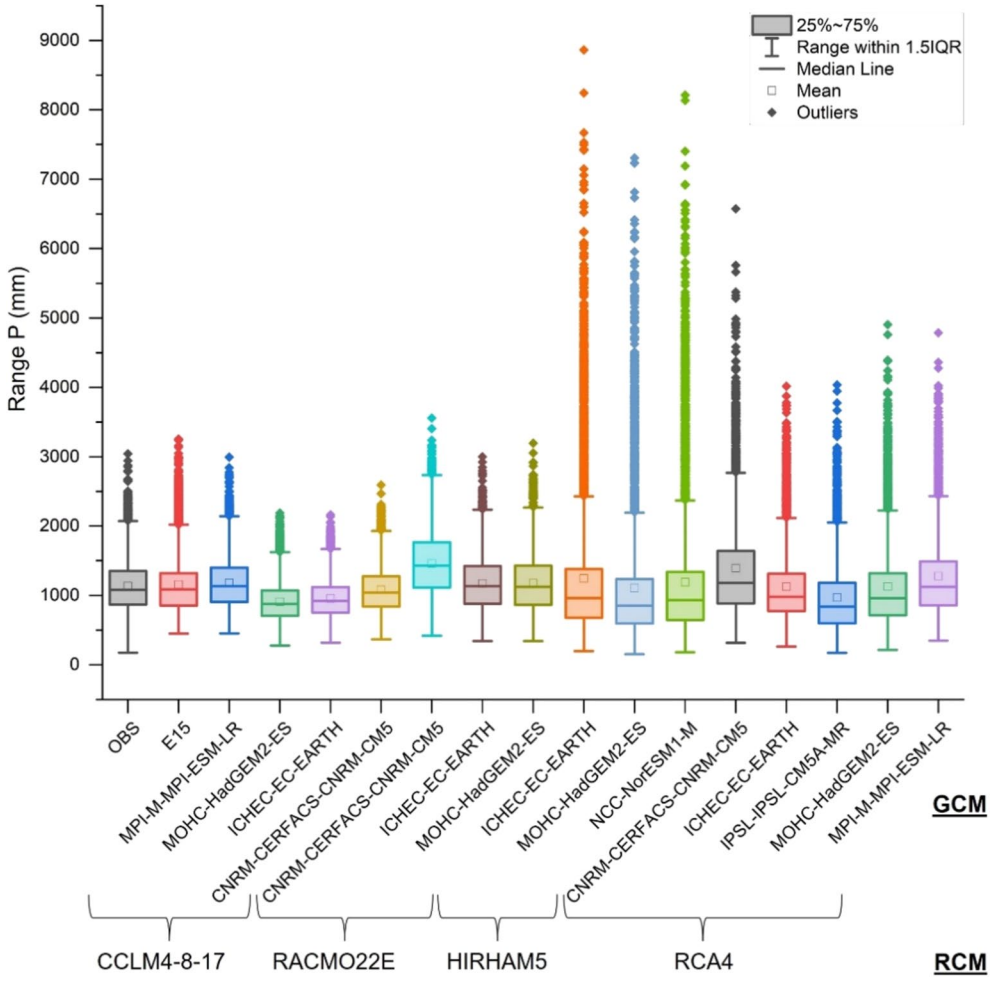

Figure 6. Box plot representing the frequency distribution of annual precipitation values of the 15 RCMs, the E15 and OBS.

inadequate representation of complex orographic areas and a wrong evaluation of the net incoming short wave radiation. Specifically, by comparing $E15_T$ and OBS_T, it was observed that in both cases the values assume a normal distribution (Fig. 8a) but that $E15_T$ underestimates observed data by about 16%.

RCM bias-correction

To investigate the future effects of climate change on groundwater recharge of the principal aquifer systems of southern Italy, the $E15_P$ and $E15_T$ were bias-corrected according to the Eq. (2) and using the results obtained with the bias inferential statistical analysis (Tables 4 and 5).

The application of the corrections leads to a significant bias reduction, being the corrected $E15_P$ overestimation of about 0.4% (Fig. 8b and c) and the corrected $E15_T$ underestimation of about 2.4% (Table 5) (Fig. 8b and c).

Hydro-climatological scenarios (2006–2100)

The annual corrected values of $E15_P$ and $E15_T$ were used to reconstruct a continuous time series until 2100, for both RCP4.5 and RCP8.5 scenarios, over the entire domain of the karst aquifers of southern Italy (Fig. 9). Precipitation projections show a decreasing trend under both pathways, with strong interannual variations and rates especially under the RCP8.5 (Fig. 10a).

Both scenarios project a relevant increase in air temperature, in particular the RCP8.5 shows the largest increase of the mean value up to about 4 °C at the end of the century (Fig. 10b) while the RCP4.5 projects an increase up to 2 °C of the mean value. The differences between scenarios are clearly recognizable from 2040, where a divergence in the trends of the time series occurs.

For $E15_P$ and $E15_T$ time series under both scenarios, a confidence interval (error) was reconstructed considering the value of the standard deviation of the bias estimated respectively in comparison to OBS_P and OBS_T, thus corresponding to a probability interval of 68.27%.

The $E15_P$ and $E15_T$ time series of both pathways were applied for quantifying the scenarios of ETR and Pe. According to the general increase in air temperature, scenarios of ETR (2006–2110) reveals a progressive rise for both RCP pathways (Fig. 11a).

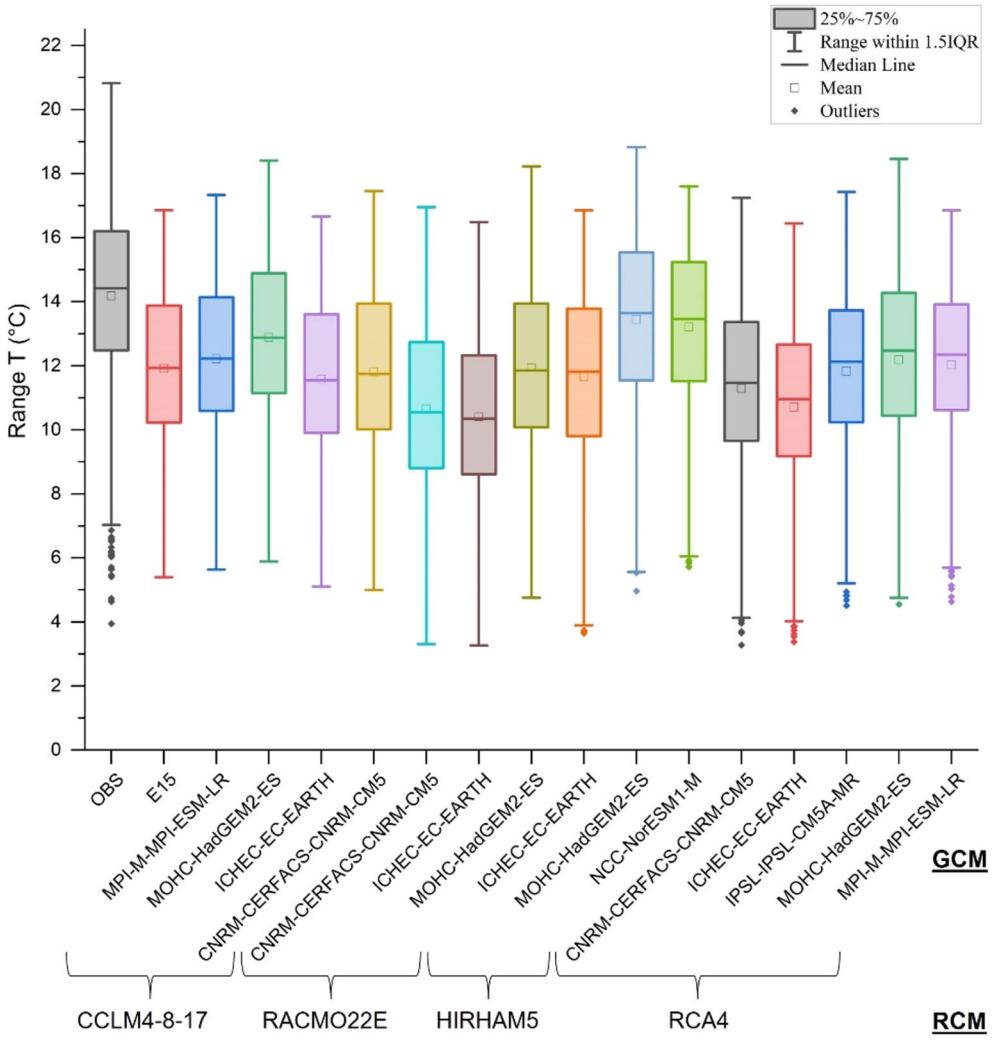

Figure 7. Box plot representing the frequency distribution of mean annual air temperature of the 15 RCMs, the E15 and OBS:

	Mean precipitation (mm)				
	OBS_P	$E15_P$	Bias $E15_P$	$E15_P$ corr	Bias $E15_P$ corr
Mean	1135.4	1157.7	**0.070**	1076.6	− 0.004
Standard deviation	368.8	429.4	0.420	399.4	0.387

Table 4. Mean annual precipitation over the period 1950–1996: observed values (OBS_P), RCM ensemble mean ($E15_P$), Bias $E15_P$ (Bias $E15_P$), $E15_P$ corrected ($E15_P$ corr), Bias $E15_P$ corrected (Bias $E15_P$ corr.). Significant values are in bold.

	Mean air temperature (°C)				
	OBS_T	$E15_T$	Bias $E15_T$	$E15_T$ corr	Bias $E15_T$ corr
Mean	14.19	11.92	**− 0.160**	13.78	− 0.024
Standard Deviation	2.63	2.57	0.120	2.970	0.143

Table 5. Mean annual air temperature over the period 1950–1996: observed values (OBS_T), RCM ensemble mean ($E15_T$), Bias $E15_T$ (Bias $E15_T$), $E15_T$ corrected ($E15_T$ corr), Bias $E15_T$ corrected (Bias $E15_T$ corr.). Significant values are in bold.

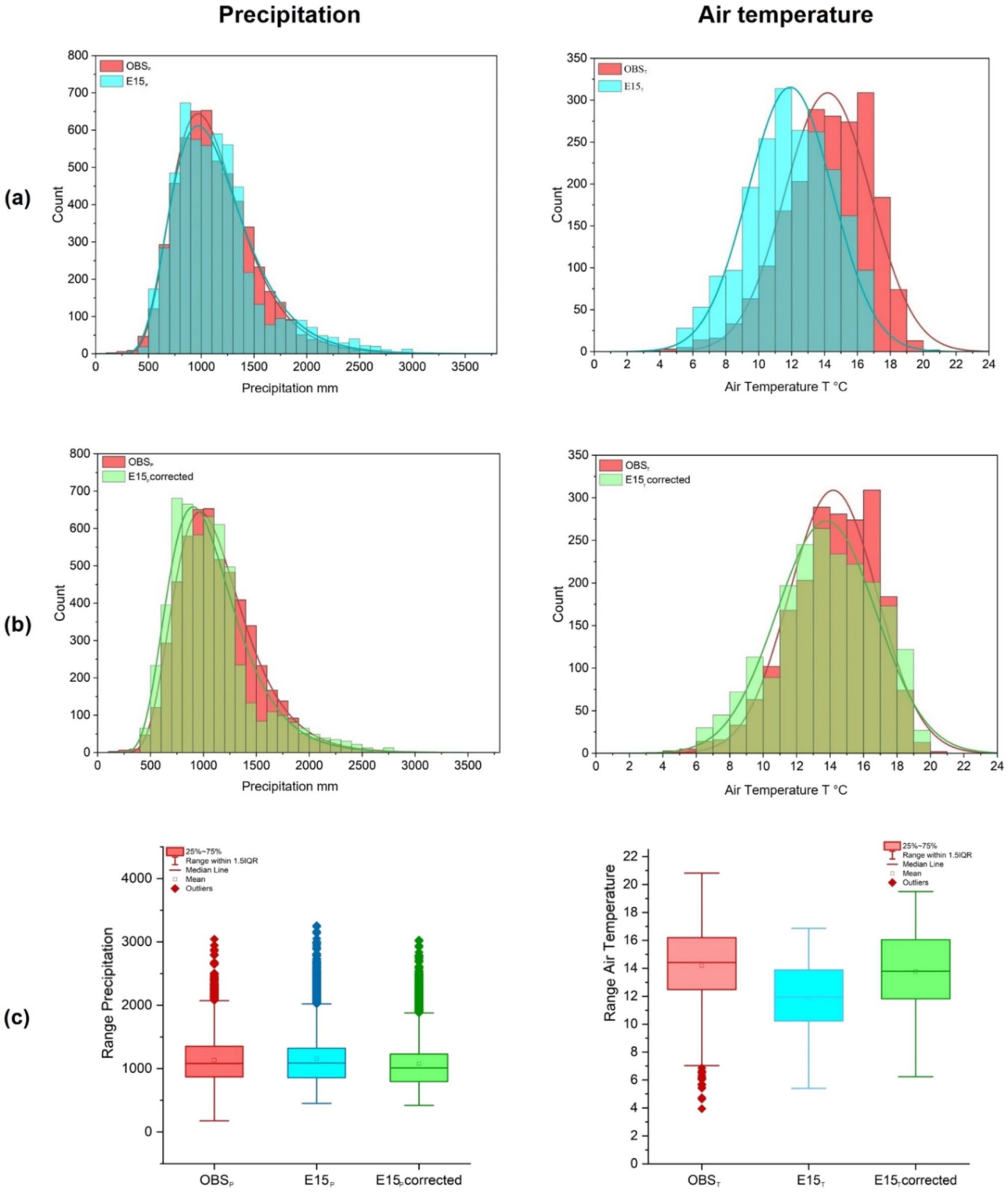

Figure 8. (**a**) Frequency distributions of OBS_P and $E15_P$ data (left) and OBS_T and $E15_T$ data (right); (**b**) frequency distributions of OBS_P and $E15_P$ data (left) and OBS_T and corrected $E15_T$ data (right); (**c**) Box plot of OBS_P, $E15_P$ and corrected $E15_P$ (left) and OBS_T, $E15_T$ and corrected $E15_T$ (right).

As a first result, Pe time series show a marked decreasing trend for both RCP8.5 and RCP4.5 pathways, with the most severe condition for the RCP8.5 one (Fig. 11b). This is clearly confirmed by the comparison of the cumulative frequency distribution (%) of Pe time series in the "historical experiment" period (1950–2005) and Pe time series of scenarios from 2045 to 2100 of both pathways (Fig. 12a); in detail, it is possible to assess that the median values (frequency of 50%) amount to 510 mm for the "historical experiment" period (1950–2005), and to 415 mm and 320 mm for RCP4.5 and RCP8.5 pathways (2006–2100), respectively.

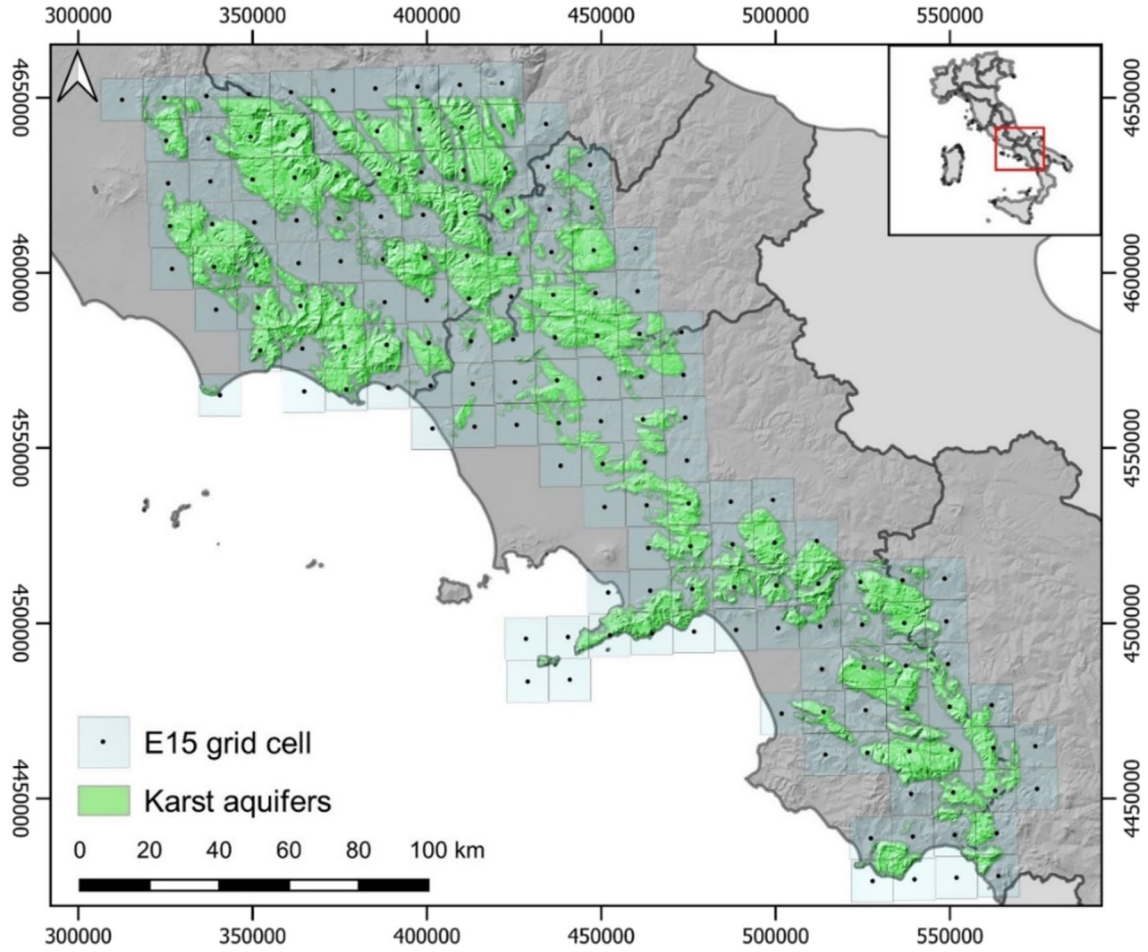

Figure 9. Map of the RCMs grid cells, comprising the domain of karst aquifers. These grid cells were considered for the calculation of $E15_P$ and $E15_T$ over the karst aquifers of southern Italy for both the "historical experiment" (1950–2005) and scenario (2005–2110) periods. The centroid of each cell is showed as a small black dot. The map was created using QGIS software (v. 3.34; https://qgis.org/).

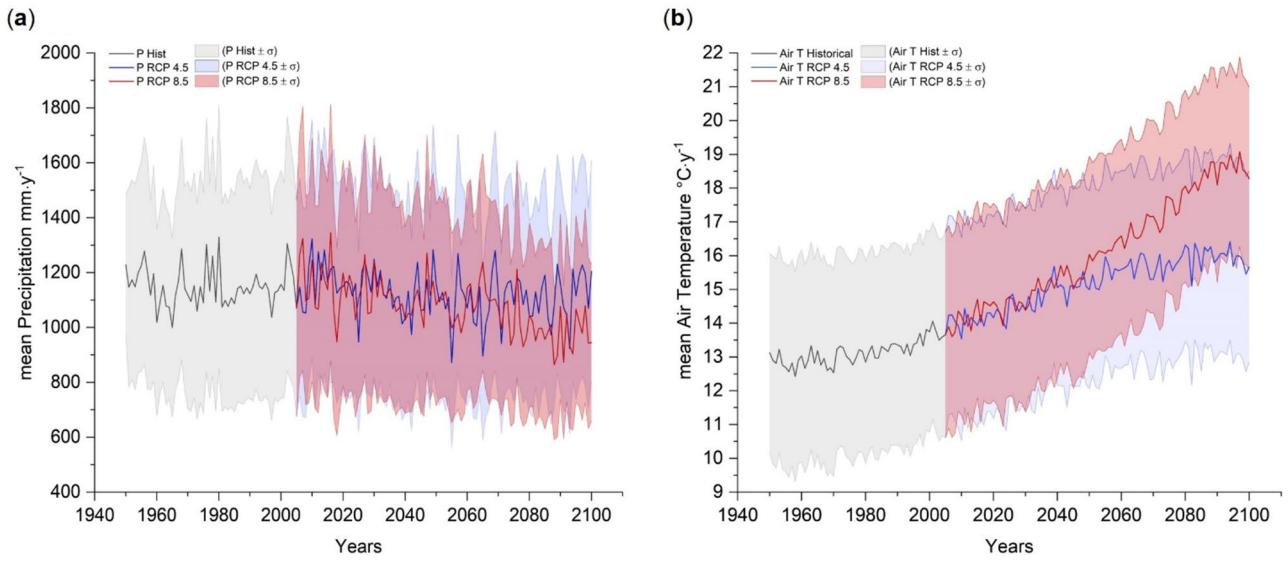

Figure 10. Time series of the "historical" period (1950–2005) and scenarios (2006–2100) under RCP8.5 and RCP4.5 pathways: (**a**) mean annual precipitation; (**b**) mean annual air temperature. Keys to symbols: for (**a**) and (**b**) the confidence interval is calculated as ± σ.

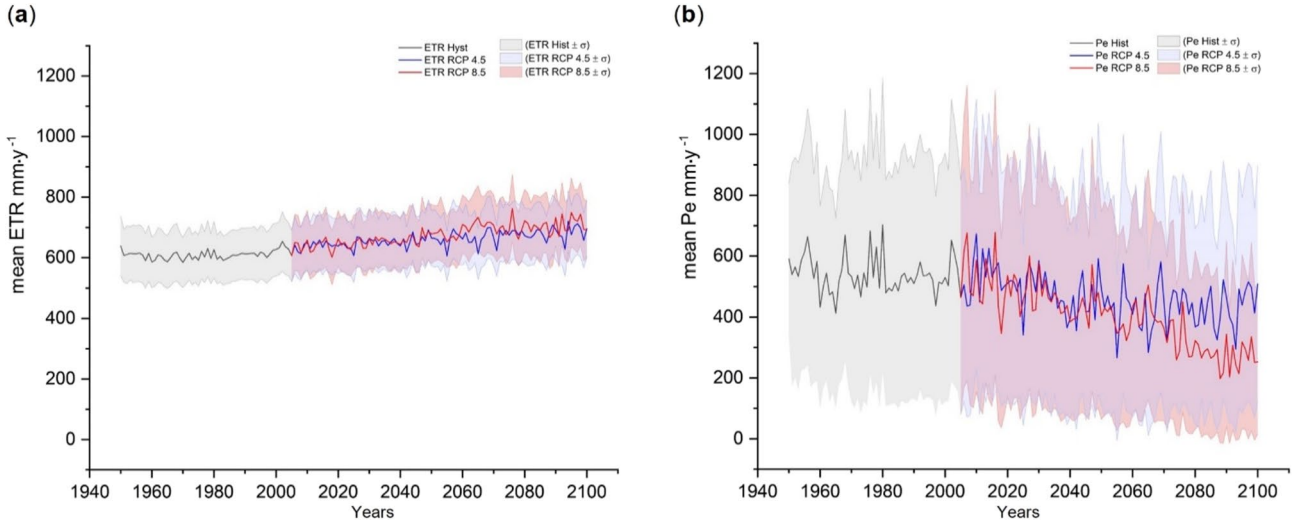

Figure 11. (**a**) Mean annual evapotranspiration ETR time series in the "historical experiment" period (1950–2005) and scenarios (2006–2110) of RCP8.5 and RCP4.5 pathways; (**b**) mean annual effective precipitation Pe time series of the "historical experiment" period (1950–2005) and scenarios (2006–2110) of RCP8.5 and RCP4.5 pathways scenarios. Keys to symbols: for (**a**) and (**b**) the confidence interval is calculated as ± σ.

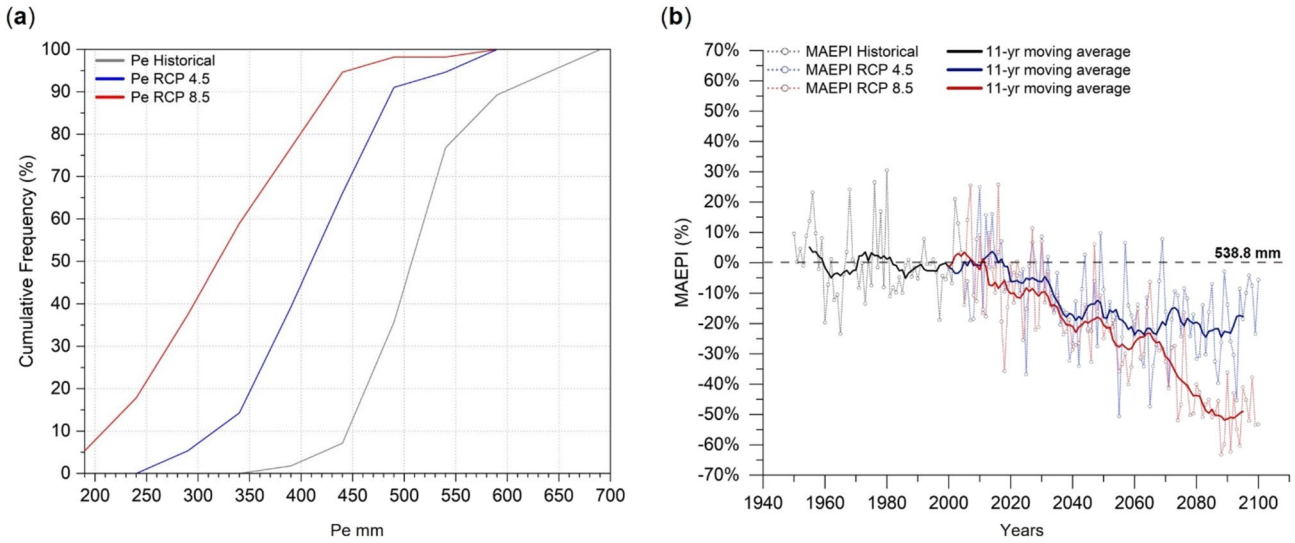

Figure 12. (**a**) cumulative frequency of Pe time series in the "historical experiment" period (1950–2005) and scenarios (2006–2110) of RCP8.5 and RCP4.5 pathways; (**b**) MAEPI time series of the "historical experiment" period (1950–2005) and scenarios (2006–2110) of RCP8.5 and RCP4.5 pathways scenarios. Keys to symbols: continuous thick lines represent 11-yrs moving average; dashed line and number (mm) represent the absolute effective precipitation (Pe) mean value of the historical period.

The trend of MAEPI shows a quite stable decadal trend in the "historical experiment" period (1950–2005), whose global average is about 538.8 mm (Fig. 12b), while relevant decreasing trends for the long-trend projections (2006–2100) of both pathways scenarios indicating a decrease of the 11-yrs moving average down to − 20% for RPC 4.5 and − 50% for RPC 8.5. In detail, the projected time series of both pathways show (starting from 2040) for the RPC 4.5 a stabilisation of the MAEPI 11-yrs moving average around a value 20% lower than the average of the "historical experiment" period (538.8 mm), and an enhancement of the decreasing trend for the RPC 8.5.

Moreover, remarkable annual and complexly cyclical fluctuations around the 11-yrs moving average of Pe were observed within the "historical experiment" period (1950–2005) and scenarios (2006–2100) periods time series (Fig. 12b).

In comparison to the Pe mean value of the whole "historical experiment" period (538.8 mm), MAEPI ranges in the "historical experiment" period from a minimum − 23.4% (1965) to a maximum + 30.47% (1980). Moreover, MAEPI showed two pluriannual phases with values above the mean value of the whole "historical experiment" period (1950–2005), corresponding respectively to periods 1955–1959 and 1971–1981, and two phases below this mean value, corresponding to the periods 1960–1970 and 1982–2000.

Similarly, MAEPI estimated for the future scenario periods (2005–2110) for both pathways RCP4.5 and RCP8.5 showed marked inter-annual fluctuations overlapping on the decreasing trends, with a fluctuation range of about ± 15% around the 11-yrs moving average, which appear reaching and exceeding the mean value of the "historical experiment" period (538.8 mm) only in few years until 2070, for the RPC 4.5 pathway scenario, and until 2040, for the PRC 8.5 one.

Discussion

In this work, an application of RCM climate models is proposed as a practical tool to assess, analyse and predict the effects of climate change until the end of the current century on the hydrological variables that control groundwater recharge processes in the principal aquifer systems of southern Italy, which are chiefly represented by karst aquifers.

Among the most relevant outcomes of this research, the ensemble of RCMs (E15) for precipitation ($E15_P$) and air temperature ($E15_T$) overperforms the representation of observed precipitation (OBS_P) and air temperature (OBS_T) data, with respect to the individual models. Data were recorded over the whole region in the Calibration period (1950–1996) by the SIMN national meteorological network, even discontinuously in space and time. According to the regional scale of analysis, needed for the hydrogeological purposes, the research was focused on the comparison of $E15_P$ and $E15_T$ to OBS_P and OBS_T in order to assess statistical differences, namely the bias between the modelled and observed data. In such a view, this work can be conceived novel in the field of application of RCMs because comparing modelled and observed meteorological data on a regional scale by accounting for the spatial and temporal discontinuity of observed time series, which is a common issue of the regional meteorological networks.

The *bias-correction* method proposed in this study is based on inferential statistical analysis of precipitation and air temperature values of both E15 and OBS data, which are discontinuous in space and time. The method proposed allows the management of OBS data aggregated at the annual scale for the estimation of the groundwater recharge, thus not requiring precipitation data aggregated at the daily or monthly time scales with continuous time series as needed for other bias-correction methods such as linear scaling (LS)[58,59], local intensity scaling (LOCI)[58,60], and the quantile mapping (QM)[59]. Moreover, the approach adopted, even being similar to the ISI-MIP method[61], due to the definition of correction coefficients based on inferential statistical analyses of modelled and observed time series at daily and monthly time scales, is innovative because considering the annual time scale and the regional scale.

The RCP 4.5 (intermediate) and RCP 8.5 (severe) scenarios used for the E15 are widely applied in studies dealing with the impact of climate change on groundwater regime in the Mediterranean area (Table 1). Under the conditions projected by the RCP8.5 scenario, the impacts of climate change on the Mediterranean region would be particularly severe with an increase in the average air temperature of several degrees by 2100[4,5].

Even though the RCP 8.5 scenario is the least likely[49], its application is justifiable because representing the most severe, thus being consistent with the precautionary principle[62].

Precipitation and air temperature rates resulting from the E15, related to scenarios of both RCP8.5 and RCP4.5 pathways, show trends consistent with those described in various climatological studies carried out in the central and southern Italy[45,57,63–65]. In the same way, MAEPI derived by E15 variables, show a complex periodicity with decadal and overlapped interannual fluctuations. Considering the calibration period (1950–1996), these complex fluctuations of both precipitation (P) and effective precipitation (Pe) were already recognized to be related to the North Atlantic Oscillation[56].

Similarly, from the predictive scenarios, it can be seen how ETR and Pe are strongly controlled by the long-term decrease in precipitation and increase in air temperature rates, especially considering the scenario regulated by the RCP8.5 pathways. In addition, the integrated analysis of MAEPI showed, by the filtering with the 11-yrs moving average, a complex periodicity of the time series with decreasing cycles until the end of the century for both RCP scenarios with a total decrease of the moving average value down to − 20% for RCP4.5 and to − 50% for RCP8.5. Given the direct correlation between effective precipitation Pe (P – ETR) and groundwater recharge[37], the future patterns of MAEPI indicate the expected variability in groundwater recharge. This is strengthened if considering the very high permeability of karst aquifers that favours chiefly infiltration in comparison to runoff.

Conclusions

The analysis of the impacts of climate change, under RCP 4.5 and RCP 8.5 scenarios, on air temperature (T), precipitation (P), actual evapotranspiration (ETR) and effective precipitation Pe (P – ETR), controlling groundwater recharge of principal aquifer systems of southern Italy, was the main focus of this study.

A methodology is presented in this study, aimed to compare and correct P and T data of an ensemble mean of 15 RCMs (E15), at 0.11° (~ 12 km) grid spatial resolution, with observed values provided by a dense meteorological network which functioned discontinuously in space and time over the period 1950–1996.

E15 data and recordings of the regional meteorological network (OBS) show similar frequency distributions of P and T, thus resulting statistically valid and comparable.

E15 projections show a reduction in precipitation and an increase in air temperature under both RCPs, with a divergence point between the two scenarios occurring by about 2040.

As a result, Pe, which is considered as a proxy of groundwater recharge, is characterized by significant inter-annual fluctuations and shows decreasing trends under both RCP scenarios, reaching a decrease of the 11-yrs moving average down to − 20%, for RCP4.5, and − 50% for the "business as usual" RCP8.5.

In summary, the proposed methodology can be considered valid for analysing the effects of climate variations at the regional scale on the selected hydrological variables (P, T, ETR and Pe) that control groundwater recharge processes of principal aquifer systems of the southern Italy, from which the socio-economic development and

environmental conservation of groundwater dependant ecosystems are reliant on. This research has revealed the potential of RCMs in the definition of groundwater recharge scenarios under future changing climate conditions, highlighting the relevant vulnerability of principal aquifer systems, among which the karst ones are the most important.

Data availability

EURO-CORDEX simulations data are publicly available upon registration from the nodes of the Earth System Grid Federation (ESGF; https://esgf.llnl.gov/) and the SIMN data of annual precipitation and mean annual temperature are freely available from the Italian Institute for Environmental Protection and Research (ISPRA) (https://www.isprambiente.gov.it/it/progetti/cartella-progetti-in-corso/acque-interne-e-marino-costiere-1/progetti-conclusi/progetto-annali). However, all raw data can be provided by the corresponding authors upon request.

Received: 27 April 2024; Accepted: 14 August 2024
Published online: 05 November 2024

References

1. Stevanović, Z. Karst aquifers in the Arid World of Africa and the Middle East: Sustainability or humanity? In *Karst Water Environment: Advances in Research, Management and Policy* 1–43 (Springer International Publishing, 2018).
2. Compagnucci, R. *et al.* Nigel Arnell (UK) and Chunzhen Liu (China). *Climate Change 2001: Impacts, Adaptation, and Vulnerability: Contribution of Working Group II to the Third Assessment Report of the Intergovernmental Panel on Climate Change* **2**, 191 (2001).
3. Huntington, T. G. Evidence for intensification of the global water cycle: Review and synthesis. *J. Hydrol.* **319**, 83–95 (2006).
4. IPCC. Summary for policymakers. *In Global Warming of 1.5°C. An IPCC Special Report on the Impacts of Global Warming of 1.5 °C above Pre-Industrial Levels and Related Global Greenhouse Gas Emission Pathways, in the Context of Strengthening the Global Response to the Threat of Climate Change, Sustainable Development, and Efforts to Eradicate Poverty* (Eds Masson-Delmotte, V., P. Zhai, H.-O. Pörtner, D. Roberts, J. Skea, P.R. Shukla, A. Pirani, W. Moufouma-Okia, C. Péan, R. Pidcock, S. Connors, J.B.R. Matthews, Y. Chen, X. Zhou, M.I. Gomis, E. Lonnoy, T. Maycock, M. Tignor, and T. Waterfield) (Cambridge University Press, 2018).
5. IPCC. *Climate Change 2014: Synthesis Report. Contribution of Working Groups I, II and III to the Fifth Assessment Report of the Intergovernmental Panel on Climate Change [Core Writing Team, R.K. Pachauri and L.A. Meyer (Eds.)]. IPCC, Geneva, Switzerland*, Pp 151 (2014).
6. Giorgi, F. Climate change hot-spots. *Geophys. Res. Lett.* **33**, 025734 (2006).
7. Giorgi, F., Jones, C. & Asrar, G. Addressing climate information needs at the regional level: the CORDEX framework. *Organ. (WMO) Bull.* **58**, 175–183 (2009).
8. Kjellström, E. *et al.* Emerging regional climate change signals for Europe under varying large-scale circulation conditions. *Clim. Res.* **56**, 103–119 (2013).
9. D'Oria, M., Tanda, M. G. & Todaro, V. Assessment of local climate change: Historical trends and RCM multi-model projections over the Salento Area (Italy). *Water (Switzerland)* **10**, 978 (2018).
10. Taylor, R. G. *et al.* Ground water and climate change. *Nat. Clim. Change* **3**, 322–329 (2013).
11. Green, T. R. *et al.* Beneath the surface of global change: Impacts of climate change on groundwater. *J. Hydrol.* **405**, 532–560 (2011).
12. Van Vuuren, D. P. *et al.* The representative concentration pathways: An overview. *Clim. Change* **109**, 5–31 (2011).
13. Fernández, J. *et al.* Consistency of climate change projections from multiple global and regional model intercomparison projects. *Clim. Dyn.* **52**, 1139–1156 (2019).
14. Holman, I. P., Allen, D. M., Cuthbert, M. O. & Goderniaux, P. Towards best practice for assessing the impacts of climate change on groundwater. *Hydrogeol. J.* **20**, 1–4 (2012).
15. Kurylyk, B. L. & MacQuarrie, K. T. B. The uncertainty associated with estimating future groundwater recharge: A summary of recent research and an example from a small unconfined aquifer in a northern humid-continental climate. *J. Hydrol.* **492**, 244–253 (2013).
16. Stigter, T. Y. *et al.* Comparative assessment of climate change and its impacts on three coastal aquifers in the Mediterranean. *Reg. Environ. Change* **14**, 41–56 (2012).
17. Stigter, T. Y. *et al.* Comparative assessment of climate change and its impacts on three coastal aquifers in the Mediterranean. *Reg. Environ. Change* **14**, 41–56 (2014).
18. Pulido-Velazquez, D., García-Aróstegui, J. L., Molina, J. & Pulido-Velazquez, M. Assessment of future groundwater recharge in semi-arid regions under climate change scenarios (Serral-Salinas aquifer, SE Spain). Could increased rainfall variability increase the recharge rate?. *Hydrol. Process.* **29**, 828–844 (2015).
19. Pulido-Velazquez, D., Collados-Lara, A. J. & Alcalá, F. J. Assessing impacts of future potential climate change scenarios on aquifer recharge in continental Spain. *J. Hydrol.* **567**, 803–819 (2018).
20. D'Oria, M., Ferraresi, M. & Tanda, M. G. Quantifying the impacts of climate change on water resources in northern Tuscany, Italy, using high-resolution regional projections. *Hydrol. Process.* **33**, 978–993 (2019).
21. Pardo-Igúzquiza, E., Collados-Lara, A. J. & Pulido-Velazquez, D. Potential future impact of climate change on recharge in the Sierra de las Nieves (southern Spain) high-relief karst aquifer using regional climate models and statistical corrections. *Environ. Earth Sci.* **78**, 1–12 (2019).
22. Nerantzaki, S. D. & Nikolaidis, N. P. The response of three Mediterranean karst springs to drought and the impact of climate change. *J. Hydrol.* **591**, 125296 (2020).
23. Voulanas, D. *et al.* Assessment of potential hydrological climate change impacts in the Kastoria basin (Western Macedonia, Greece) using EURO-CORDEX regional climate models. Zollo A. *Int. J. Climatol.* **36**, 987–1004 (2021).
24. IPCC. Towards new scenarios for analysis of emissions, climate change, impacts, and response strategies. IPCC EXPERT MEETING REPORT. *Clim. Change Impacts Response Strat.*, **132** (2008).
25. Jacob, D. *et al.* EURO-CORDEX: New high-resolution climate change projections for European impact research. *Reg. Environ. Change* **14**, 563–578 (2014).
26. Moss, R. H. *et al.* The next generation of scenarios for climate change research and assessment. *Nature* **463**, 747–756 (2010).
27. Sulis, M., Paniconi, C., Marrocu, M., Huard, D. & Chaumont, D. Hydrologic response to multimodel climate output using a physically based model of groundwater/surface water interactions. *Water Resour. Res.* https://doi.org/10.1029/2012WR012304 (2012).
28. Teutschbein, C. & Seibert, J. Bias correction of regional climate model simulations for hydrological climate-change impact studies: Review and evaluation of different methods. *J. Hydrol.* **456–457**, 12–29 (2012).
29. Gudmundsson, L., Bremnes, J. B., Haugen, J. E. & Engen-Skaugen, T. Hydrology and earth system sciences technical note: Downscaling RCM precipitation to the station scale using statistical transformations-a comparison of methods. *Hydrol. Earth Syst. Sci.* **16**, 3383–3390 (2012).

30. De Vita, P. *et al.* Hydrogeology of continental southern Italy. *J. Maps* **14**, 230–241 (2018).
31. Bonardi, G. *et al.* Carta delle principali unità cinematiche dell'appennino meridionale. Nota illustrative. *Boll. della Soc. Geol. Ital.* **128**, 47–60 (2009).
32. Mostardini, F. & Merlini, S. Appennino centro meridionale, sezioni geologiche e proposta di modello strutturale. [Central-southern Apennine, geological crosssections and proposal of a structural model. *Mem. Soc. Geol. Ital.* **35**, 177–202 (1986).
33. Ruggieri, G. *et al.* Testing evapotranspiration estimates based on MODIS satellite data in the assessment of the groundwater recharge of karst aquifers in southern Italy. *Water* **13**, 118 (2021).
34. Celico, P. B. Idrogeologia dei massicci carbonatici, delle piane quaternarie e delle aree vulcaniche dell Italia centro-meridionale (Marche e Lazio meridionali, Abruzzo, Molise e Campania). *Idrogeologia dei massicci carbonatici, delle piane quaternarie e delle aree vulcaniche dell Italia centro-meridionale (Marche e Lazio meridionali, Abruzzo, Molise e Campania)* **4/2**, 1–225 (1983).
35. Petrella, E., Aquino, D., Fiorillo, F. & Celico, F. The effect of low-permeability fault zones on groundwater flow in a compartmentalized system. Experimental evidence from a carbonate aquifer (Southern Italy). *Hydrol. Process.* **29**, 1577–1587 (2015).
36. Allocca, V., De Vita, P., Manna, F. & Nimmo, J. R. Groundwater recharge assessment at local and episodic scale in a soil mantled perched karst aquifer in southern Italy. *J. Hydrol.* **529**, 843–853 (2015).
37. Allocca, V., Manna, F. & De Vita, P. Estimating annual groundwater recharge coefficient for karst aquifers of the southern Apennines (Italy). *Hydrol. Earth Syst. Sci.* **18**, 803–817 (2014).
38. Fusco, F., Allocca, V. & De Vita, P. Hydro-geomorphological modelling of ash-fall pyroclastic soils for debris flow initiation and groundwater recharge in Campania (southern Italy). *Catena* **158**, 235–249 (2017).
39. Cusano, D. *et al.* A comparison of methods for assessing groundwater vulnerability in karst aquifers: The case study of Terminio Mt. aquifer (Southern Italy). *Sustain. Environ. Res.* **33**, 42 (2023).
40. Tufano, R. *et al.* Groundwater vulnerability of principal aquifers of the Campania region (southern Italy). *J. Maps* **16**, 565–576 (2020).
41. Allocca, V. *et al.* Hydrogeological and hydrogeochemical study of a volcanic-sedimentary coastal aquifer in the archaeological site of Cumae (Phlegraean Fields, southern Italy). *J. Geochem. Explor.* **185**, 105–115 (2018).
42. Cusano, D. *et al.* The survey of Italian springs by the National Hydrographic Service, a forgotten database. Structuring and analysis of a dataset of Campania springs (southern Italy). *AS-ITJGW* **11**, 31–41 (2022).
43. Olarinoye, T. *et al.* Global karst springs hydrograph dataset for research and management of the world's fastest-flowing groundwater. *Sci. Data* **7**, 59 (2020).
44. Bucchignani, E., Mercogliano, P., Panitz, H.-J. & Montesarchio, M. Climate change projections for the Middle East-North Africa domain with COSMO-CLM at different spatial resolutions. *Adv. Clim. Change Res.* **9**, 66–80 (2018).
45. Bucchignani, E., Montesarchio, M., Zollo, A. L. & Mercogliano, P. High-resolution climate simulations with COSMO-CLM over Italy: Performance evaluation and climate projections for the 21st century. *Int. J. Climatol.* **36**, 735–756 (2016).
46. Bucchignani, E., Montesarchio, M., Cattaneo, L., Manzi, M. P. & Mercogliano, P. Regional climate modeling over China with COSMO-CLM: Performance assessment and climate projections. *J. Geophys. Res. Atmos.* **119**, 12–151 (2014).
47. Spinoni, J. *et al.* Future global meteorological drought hot spots: A study based on CORDEX data. *J. Clim.* **33**, 3635–3661 (2020).
48. Zittis, G. *et al.* Business-as-usual will lead to super and ultra-extreme heatwaves in the Middle East and North Africa. *NPJ Clim. Atmos. Sci.* **4**, 20 (2021).
49. Hausfather, Z. & Peters, G. P. Emissions–the 'business as usual'story is misleading. *Nature* **577**, 618–620 (2020).
50. Schulzweida, U. CDO user guide. Zenodo https://doi.org/10.5281/zenodo.7112925 (2022).
51. Trzaska, S. & Schnarr, E. A review of downscaling methods for climate change projections. *United States Agency for International Development by Tetra Tech ARD*, 1–42 (2014).
52. Shaw, E., Beven, K. J., Chappell, N. A. & Lamb, R. *Hydrology in Practice* (CRC Press, 2010).
53. Turc, L. L. Bilan d'eau des sols: Relations entre les précipitations, l'évaporation et l'écoulement. *Journées de l'hydraulique* **3**, 36–44 (1955).
54. Coutagne, A. Quelques considérations sur le pouvoir évaporant de l'atmosphère, le déficit d'écoulement effectif et le déficit d'écoulement maximum. *La Houille Blanche* **40**, 360–374 (1954).
55. Thornthwaite, C. W. The water balance. *Climatology* **8**(1), 1–104 (1955).
56. De Vita, P., Allocca, V., Manna, F. & Fabbrocino, S. Coupled decadal variability of the North Atlantic Oscillation, regional rainfall and karst spring discharges in the Campania region (southern Italy). *Hydrol. Earth Syst. Sci.* **16**, 1389–1399 (2012).
57. Zollo, A. L., Rillo, V., Bucchignani, E., Montesarchio, M. & Mercogliano, P. Extreme temperature and precipitation events over Italy: Assessment of high-resolution simulations with COSMO-CLM and future scenarios. *Int. J. Climatol.* **36**, 987–1004 (2016).
58. Schmidli, J., Frei, C. & Vidale, P. L. Downscaling from GCM precipitation: A benchmark for dynamical and statistical downscaling methods. *Int. J. Climatol.* **26**, 679–689 (2006).
59. Wetterhall, F., Pappenberger, F., He, Y., Freer, J. & Cloke, H. Conditioning model output statistics of regional climate model precipitation on circulation patterns. *Nonlinear Process. Geophys.* **19**, 623–633 (2012).
60. Themeßl, M. & Gobiet, A. Empirical-statistical downscaling and model error correction of daily temperature and precipitation from regional climate simulations and the effects on climate change signals. In *Proc. of the EGU General Assembly, Vienna, Austria*, 2–7 (2010).
61. Hempel, S., Frieler, K., Warszawski, L., Schewe, J. & Piontek, F. A trend-preserving bias correction—The ISI-MIP approach. *Earth Syst. Dyn.* **4**, 219–236 (2013).
62. Ricci, P. F. & Sheng, H. *Benefits and Limitations of the Precautionary Principle* (Elsevier, 2013).
63. D'Oria, M., Balacco, G., Todaro, V., Alfio, M. R. & Tanda, M. G. Assessing the impact of climate change on a coastal karst aquifer in a semi-arid area. *Groundw. Sustain. Dev.* **25**, 101131 (2024).
64. Alfio, M. R., Pisinaras, V., Panagopoulos, A. & Balacco, G. A comprehensive assessment of RCP4.5 projections and bias-correction techniques in a complex coastal karstic aquifer in the Mediterranean. *Front. Earth Sci.* **11**, 1231296 (2023).
65. Braca, G., Bussettini, M., Ducci, D., Lastoria, B. & Mariani, S. Evaluation of national and regional groundwater resources under climate change scenarios using a GIS-based water budget procedure. *Rend. Lincei. Sci. Fis. Nat.* **30**, 109–123 (2019).

Acknowledgements

Authors acknowledge the funding of the research by the PhD Program of Dipartimento di Scienze della Terra, dell'Ambiente e delle Risorse (DiSTAR), Università di Napoli Federico II (36th cycle). The research was funded by European Union—NextGenerationEU—Mission 4 "Education and Research"—Component 2 "From Research to Business" – Investment 3.1 "Fund for the realization of an integrated system of research and innovation infrastructures"—Project IR0000037 — CUP I53C22000800006 — GeoSciences IR.

Author contributions

D.L. conceptualization, data curation, formal analysis, investigation, methodology, software, validation, visualization, writing – original draft and writing – review & editing. E.B. conceptualization, data curation, formal

analysis, investigation, methodology, validation and writing – review & editing. M.M. conceptualization, data curation, formal analysis, investigation, methodology, software, validation and writing – review & editing. V.A. conceptualization, data curation, formal analysis, investigation, methodology, validation, writing – original draft and writing – review & editing. D.C. and S.C. conceptualization, data curation, formal analysis, investigation, methodology, software, validation and writing – review & editing. P.D.V. conceptualization, data curation, formal analysis, investigation, methodology, software, validation, writing – original draft, writing – review & editing, project administration.

Competing interests

The authors declare no competing interests.

Additional information

Correspondence and requests for materials should be addressed to D.L.

Reprints and permissions information is available at www.nature.com/reprints.

Publisher's note Springer Nature remains neutral with regard to jurisdictional claims in published maps and institutional affiliations.